# Effect of resonant magnetic perturbations on three dimensional equilibria in the Madison Symmetric Torus reversed-field pinch

S. Munaretto, B. E. Chapman, M. D. Nornberg, J. Boguski, A. M. DuBois, A. F. Almagri, and J. S. Sarff

Citation: Physics of Plasmas **23**, 056104 (2016); doi: 10.1063/1.4943524
View online: http://dx.doi.org/10.1063/1.4943524
View Table of Contents: http://scitation.aip.org/content/aip/journal/pop/23/5?ver=pdfcov
Published by the AIP Publishing

# Effect of resonant magnetic perturbations on three dimensional equilibria in the Madison Symmetric Torus reversed-field pinch

S. Munaretto,[a),b)] B. E. Chapman, M. D. Nornberg, J. Boguski, A. M. DuBois, A. F. Almagri, and J. S. Sarff
*Department of Physics, University of Wisconsin–Madison, 1150 University Ave, Madison, Wisconsin 53706, USA*

(Received 30 November 2015; accepted 25 January 2016; published online 11 March 2016)

The orientation of 3D equilibria in the Madison Symmetric Torus (MST) [R. N. Dexter *et al.*, Fusion Technol. **19**, 131 (1991)] reversed-field pinch can now be controlled with a resonant magnetic perturbation (RMP). Absent the RMP, the orientation of the stationary 3D equilibrium varies from shot to shot in a semi-random manner, making its diagnosis difficult. Produced with a poloidal array of saddle coils at the vertical insulated cut in MST's thick conducting shell, an $m = 1$ RMP with an amplitude $b_r/B \sim 10\%$ forces the 3D structure into any desired orientation relative to MST's diagnostics. This control has led to improved diagnosis, revealing enhancements in both the central electron temperature and density. With sufficient amplitude, the RMP also inhibits the generation of high-energy (>20 keV) electrons, which otherwise emerge due to a reduction in magnetic stochasticity in the core. Field line tracing reveals that the RMP reintroduces stochasticity to the core. A $m = 3$ RMP of similar amplitude has little effect on the magnetic topology or the high-energy electrons. © *2016 AIP Publishing LLC*. [http://dx.doi.org/10.1063/1.4943524]

## INTRODUCTION

Application of an externally applied magnetic field with the same poloidal and toroidal mode number as a mode resonant inside a magnetically confined plasma has become an important control tool for a variety of magnetic configurations. The resonant magnetic perturbation (RMP) is used routinely in the tokamak,[1–12] the stellarator,[13,14] the heliotron,[15,16] and the reversed-field pinch (RFP).[17–21] The resonant magnetic perturbation is also considered to be of fundamental importance for the ITER tokamak advanced scenario.[3,11,22,23]

Resonant magnetic perturbations are used, e.g., for the control of ELMs, the stabilization of detached plasmas, the suppression of high-energy electrons, and the control of tearing mode rotation. The latter two are of particular importance in RFP devices when the configuration evolves from 2D (toroidally axisymmetric) to 3D (helical, stellarator like). Here, the normally broad spectrum of $m = 1$ tearing modes, called the multiple helicity (MH) state, condenses to the quasi-single-helicity (QSH) state, wherein the $m = 1$ spectrum is dominated by a single core-resonant mode, and energy confinement is improved.[24] The transition is more prevalent at higher toroidal plasma current and lower density with evidence across devices that the threshold condition may be described as either a Lundquist number or Hartmann number dependence.[25,26]

While the QSH state is common in RFP plasmas, a complete understanding of its emergence and confinement physics is still lacking. Possible explanations for its emergence have derived from visco-resistive MHD,[27–31] reconnection due to pressure-driven modes,[32] and the physics of transport barriers,[33,34] but detailed comparisons to experimental data are required. Understanding both the emergence and confinement physics of the 3D state requires measurements of profiles in the plasma core such as magnetic field, flow, and temperature.

Complete diagnosis of a helical structure already presents a significant challenge for a stationary diagnostic set given the strong geometric variation of flux surfaces. This would be ameliorated were the structure to have a finite rotation rate, but in the Madison Symmetric Torus (MST)[35] RFP, the helical structure slows and locks as it grows, and the locking orientation varies only semi-randomly from shot to shot.

To facilitate diagnosis in MST, a resonant magnetic perturbation is applied to control the orientation of the 3D structure. This has allowed an initial study in MST of the thermal electron confinement properties, one focus of this paper. This study is further facilitated by a recent advance with the 3D equilibrium reconstruction code, V3FIT.[36] Through its apparent effect on the central magnetic topology, the RMP has also allowed further examination of the confinement of high energy electrons that emerge as the 3D structure forms.[37] A RMP of sufficient amplitude suppresses these electrons, which is interpreted as a reintroduction of stochasticity to the central region. This supports the model in Clayton *et al.* wherein the high-energy electrons emerge due to a local reduction in stochasticity.[37] The physics of the emergence of this state will be addressed in future work.

The paper is organized as follows. The Experimental Setup section presents the MST device and the RMP technique.[21] The QSH characterization section describes the transition to a helical configuration in terms of electron density and temperature profiles mapped to helical flux surfaces with V3FIT. Following this is a description of the x-ray emission that reflects the presence of high-energy electrons within the helical region. This is followed by data illustrating the impacts on the electrons of both $m = 1$ and $m = 3$ magnetic

Note: Paper PI3 4, Bull. Am. Phys. Soc. **60**, 262 (2015).
[a)]Invited speaker.
[b)]smunaretto@wisc.edu

 

perturbations. The Field line tracing reconstructions section explains these impacts in terms of the effect on the magnetic topology.

## EXPERIMENTAL SETUP

The MST device is characterized by a major radius $R_0 = 1.5$ m and a minor radius $a = 0.52$ m. A 5-cm-thick conducting shell comprised of aluminum fits closely around the plasma. The conducting shell, which also serves as the vacuum vessel, has a vertical insulated cut to allow inductive drive of the toroidal plasma current. A schematic of the bottom half of the shell is shown in Figure 1. The vertical cut, located on the left in the figure, produces strong error fields that are counteracted by an active feedback system comprised of 32 sensing coils and 38 correction coils.[21] The core-resonant $m = 1$ tearing modes typically rotate spontaneously in MST. When the core-resonant mode associated with the QSH structure grows to large amplitude, it induces substantial eddy current in the shell. The eddy current is resonant with the dominant mode and produces a rotating magnetic perturbation which has a phase lag due to the finite self-inductance and resistance of the shell. The interaction of this perturbation with the core-resonant mode results in an electromagnetic drag torque that slows mode rotation until the mode locks to one of many small, static error fields.[38] To reliably stimulate the QSH transition, plasmas with a current of $I_p \simeq 500$ kA and density of $5 \times 10^{18}$ m$^{-3}$ are produced. The current required by the correction coils to counteract the error fields produced by these plasmas exceeds the system limit at a specific poloidal location. The resulting static error field sometimes causes the mode to lock with preference to a particular orientation.

Hence, measurements of the stationary 3D structure in various orientations with fixed diagnostics are very challenging. To overcome this problem, a system for locking the QSH structure into a pre-programmed orientation (phase) through the use of a resonant magnetic perturbation has been developed.[21] The technique takes advantage of the active feedback system. To achieve a particular orientation of the 3D structure, we introduce an offset in the correction of the $m = 1$ component that couples with the dominant $m = 1$, $n = 5$ tearing mode. The applied error field acts as a resonant magnetic perturbation that exerts a braking torque on the helical structure. Using this technique, the desired poloidal phase of the QSH structure can be achieved within 5° at about a $1\sigma$ confidence level when the applied perturbation has an amplitude of $B_r^{(m=1)}/B(a) \geq 8\%$.[21]

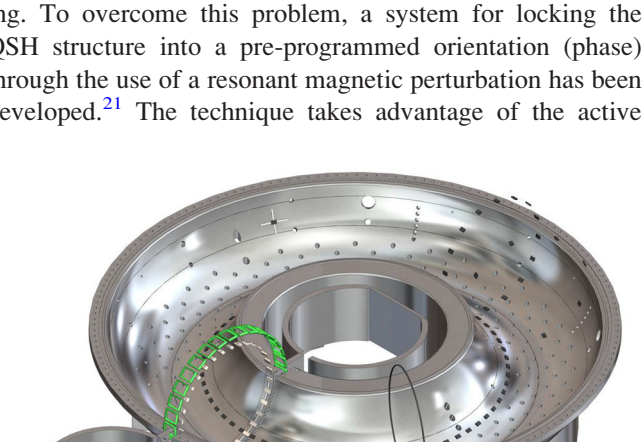

FIG. 1. Bottom half of the 5-cm-thick MST conducting shell. Located at the single vertical cut in the shell (on the left in the figure) are the error field correction coils (green) and the error field sensing coils (white). Other magnetic sensors are shown in black.

## QSH CHARACTERIZATION

The possibility of locking the helix in any desired orientation allows us to position it favorably for MST's major diagnostics, including Thomson scattering,[39] far infrared (FIR) interferometry/polarimetry,[40] and soft-x-ray (SXR) tomography.[41,42] The importance of controlling the orientation of the helical structure can be seen in Figure 2. Here, there are two different electron temperature profile measurements. The Thomson scattering system allows measurement of the electron temperature ($T_e$) along the minor radius, from near the geometric axis to the bottom of the vessel. The two measurements shown in Figure 2 are performed with the helix aligned (a) and counter-aligned (b) with the beamline of the diagnostic. The profile on the left reveals a temperature structure, consistent with experimental observations from other RFP devices.[43] The profile on the right completely misses the temperature structure. Similar considerations for the other diagnostics lead to a determination of the optimum phase of the 3D structure.

### Equilibrium reconstructions

To better understand these 3D equilibria, it is necessary to perform non-axisymmetric flux-surface reconstructions. One tool for such reconstructions is a code called NCT-SHEq[44,45] that computes an axisymmetric equilibrium and superimposes on it a perturbation with the periodicity of the innermost resonant tearing mode. External magnetic measurements constrain the equilibrium as well as the phase and amplitude of the core mode. NCT-SHEq has been used, for example, to perform a density inversion to highlight the transition to the helical magnetic equilibrium.[46]

A more advanced 3D-flux-surface reconstruction tool is the V3FIT code.[36] It reconstructs flux surfaces based on both

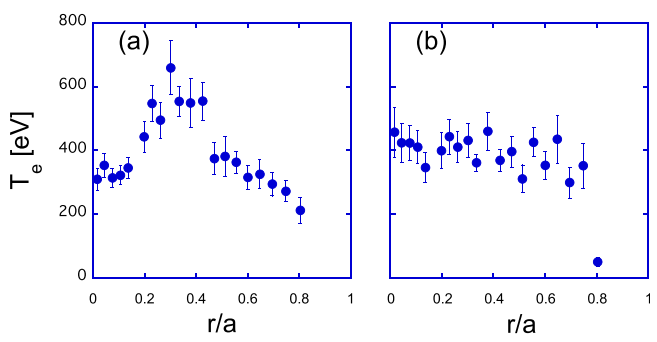


FIG. 2. On the left (a), an electron temperature profile measured when the 3D structure is aligned with the Thomson scattering beamline. On the right (b), the structure is displaced poloidally 180° from the beamline.

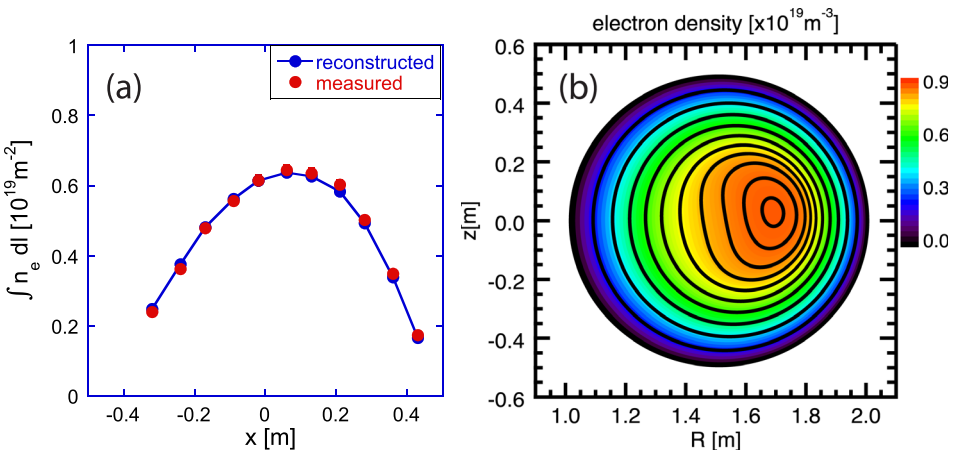


FIG. 3. On the left (a), a comparison of line-integrated density measured with the FIR interferometer to that reconstructed by V3FIT. The error bars for the measurements are of the size of the symbols. On the right (b), the density profile is mapped to the helical flux surfaces reconstructed by V3FIT.

external and internal measurements of quantities that affect the magnetic equilibrium. V3FIT has been applied to stellarator, tokamak, and RFP plasmas.[47] The code determines the best fit of a Variational Moments Equilibrium Code (VMEC) equilibrium[48] constrained by all available measurements. In MST, data from external magnetic measurements, FIR interferometry/polarimetry, Thomson scattering, and SXR tomography are included in the fit. A further improvement to the V3FIT reconstructions for MST has been recently achieved by including the contribution of the edge helical perturbation from the eddy current induced in the shell.[49] Figure 3 shows an example of a reconstruction with V3FIT. A comparison of measured and reconstructed line-integrated densities is shown on the left (a). The agreement is quite good. On the right (b), the density profile is mapped onto helical flux surfaces, showing that the largest density, $\simeq 10^{19}\,\mathrm{m}^{-3}$, occurs in the center of the helical structure. A limitation in the V3FIT reconstructions comes from the assumption made in the VMEC equilibrium code. It assumes closed, nested flux surfaces and thus can only model a single magnetic axis. This limitation however is not impacting the results presented here. In the QSH state, the equilibrium is 3D around a single helical axis when the amplitude of the toroidal component of the innermost resonant mode exceeds 3.5% of the magnetic field amplitude at the edge.[43] For example, for the shot in Figure 4, this threshold corresponds to $\delta b_t^{(1,5)} = 55\,\mathrm{G}$.

### Thermal electron time evolution and high energy electron generation

A time series of electron density and temperature profiles is created from within a single discharge by reconstructing flux surfaces at a frequency of 1.5 kHz, the rate at which $T_e$ measurements are made. From these time series, we can characterize the evolution of any structures associated with the thermal electrons. In Figure 4(a), the time evolution of the amplitude of the innermost resonant mode ($m = 1$, $n = 5$) is shown. The growth of this mode is accompanied by a rise in temperature in the central part of the plasma (Figure 4(b)). But this enhancement fluctuates, as was previously observed in RFX-mod.[50] There is also a central accumulation of the electron density $n_e$ (Figure 4(c)), which in contrast to the temperature is steady and persists to the end of the QSH phase.

During the transition to QSH, a population of high-energy (runaway) electrons emerges, as indicated by the emission of high-energy x rays (bremsstrahlung).[37] This is unusual in the typically stochastic RFP plasma, since the rate of electron loss increases with electron velocity. From field line tracing with the ORBIT code,[51] it was previously hypothesized that the electron population could emerge due to a localized region of reduced stochasticity corresponding to the 3D structure.[37] However, the experimental evidence to support this picture in detail was lacking. Data presented in this and RMP impact on non-thermal and thermal electrons sections bolster this earlier hypothesis, as will be summarized in the Conclusion section of this paper.

For the present work, x-ray measurements have been made with a new detector which can count individual photons with high time response.[52] In Figure 5 on the left, x rays emitted by high-energy electrons during and after the QSH growth phase are shown. The temporal evolution of the $n = 5$ and $n = 6$ modes are shown in Figure 5(a), while the x-ray count rate is shown in Figure 5(b). The data are plotted versus relative

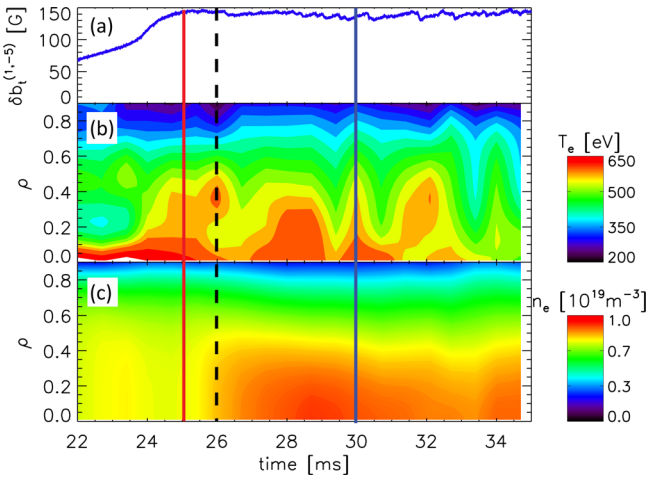


FIG. 4. Time evolution of the amplitude of the innermost resonant tearing mode (a), the electron temperature profile (b), and the electron density profile (c). The two profiles are plotted versus helical flux coordinate (vertical axis), where the 0 corresponds to the helical magnetic axis, computed with V3FIT. Discrete reconstructions versus time are smoothed to produce the continuous contour plots in the figure. Vertical dashed line indicates when the (4%) RMP is turned off. The red and blue lines indicate times when the samples of $T_e$ in Figure 8 are chosen.

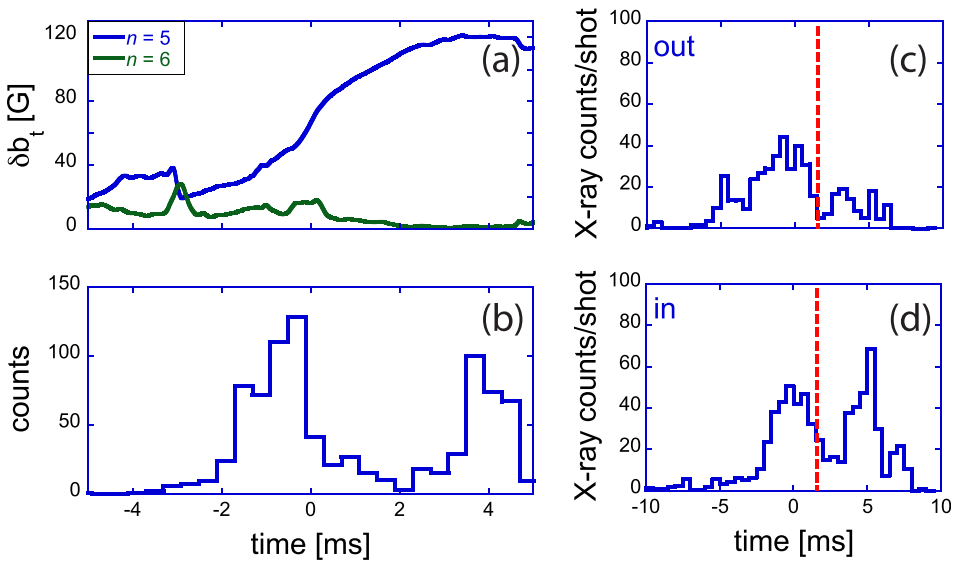


FIG. 5. Temporal evolution in a single shot of $n=5$ and $n=6$ mode amplitudes (a), x-ray count rate, including only x rays above 20 keV and binning in 0.5 ms time intervals (b). Relative time $t=0$ corresponds to $\delta b_t^{(1,5)} = 60$ G. Temporal evolution of x-ray counts averaged over multiple shots where the helical structure locks out of (c) or in (d) the detector's line of sight. The vertical dashed line at 1.5 ms indicates average time at which the $n=5$ structure locks.

time, where $t=0$ corresponds to the time when $\delta b_t^{(1,5)} = 60$ G. The x rays counted here have an energy of at least 20 keV, and the count rate is determined in 0.5 ms intervals.

The two plots on the right in Figure 5 show the difference in detected x-ray emission when the helical magnetic axis (center of the 3D structure) is locked out of (Figure 5(c)) or in (Figure 5(d)) the detector's line of sight. The data in each of these two plots were compiled from multiple similar shots without the RMP. The precise locking time of the 3D structure varies slightly from shot to shot, but on average it is at about 1.5 ms (relative time) in both cases. Before this time, while the dominant mode is still growing and rotating, the x-ray emission in the two cases is similar, as expected from data shown in Clayton *et al.*[37] After locking, however, the x-ray flux is larger when the structure is in the detector's line of sight (Figure 5(d)). This supports the earlier hypothesis that the energetic electrons are concentrated within the 3D structure.

The transition to a QSH state impacts also the confinement of fast ions, as described in Ref. 53. Here, it is shown that the helical equilibrium introduces neoclassical effects that reduce the fast ion confinement time with respect to the MH state. Despite a degradation of the fast ion confinement time, it is still larger than the one expected for stochastic transport.

## RMP IMPACT ON NON-THERMAL AND THERMAL ELECTRONS

While an external magnetic perturbation can control the orientation of the helical structure, there are additional impacts as well. The most obvious is the suppression of x-ray flux associated with the high-energy electrons, Figure 6. Here, a magnetic perturbation with $m=1$ is applied from 20 to 25 ms. Each plot corresponds to an ensemble of tens of discharges with an RMP amplitude ranging from $b_r^{RMP}/B(a) \simeq 6\% - 12\%$. As the RMP amplitude increases, the x-ray counts decrease, and with the largest-amplitude RMP's, the x-ray counts remain low after the RMP is turned off.

The suppression of the high-energy electrons with an $m=1$ magnetic perturbation is a resonant effect, depending on the presence of finite-amplitude $m=1$ modes pre-existing in the plasma. This is determined by applying a $m=3$ perturbation with an amplitude comparable to that of the $m=1$ perturbation, Figure 7. While there are $m=3$ resonant surfaces in the RFP plasma, e.g., $m=3$, $n=15$, the associated modes are of negligible amplitude compared to the $m=1$ modes. The top plot in Figure 7 shows the average x-ray count rate from a series of discharges where a $m=1$ perturbation was applied from 20 to 25 ms. The bottom plot shows the same measurement when a $m=3$ perturbation of the

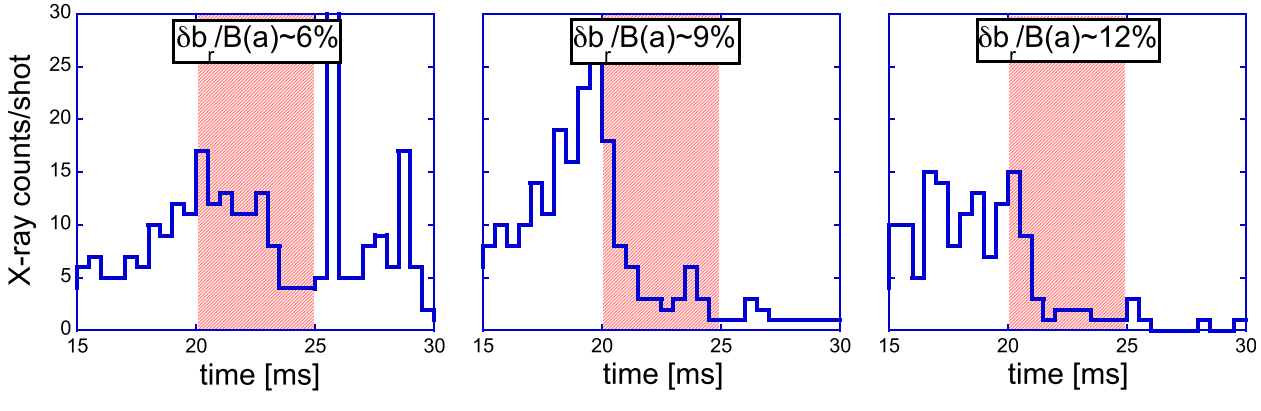


FIG. 6. Effect of $m=1$ magnetic perturbation on the high-energy electron population. X-ray counts are shot averaged in each time bin. Shaded area corresponds to the time when the RMP is applied. Normalized RMP amplitude indicated in each plot.

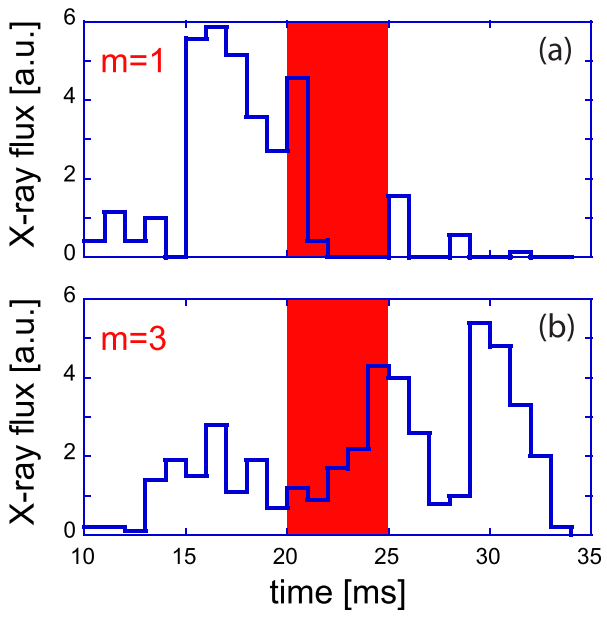


FIG. 7. Comparison of x-ray counts with $m=1$ (a) and $m=3$ (b) magnetic perturbations. Shaded areas correspond to time when perturbations are applied. Counting rate lower than in previous plots due to x-ray detector being mounted at a different location.

same amplitude is applied. It is clear that high-energy x rays are not suppressed by the $m=3$ perturbation.

There is also an apparent impact of the $m=1$ magnetic perturbation on the bulk electron temperature profile. Figure 4 showed a case with the RMP amplitude of 4% applied until 26 ms (highlighted by the dashed line). Figure 8 shows two $T_e$ radial profiles measured during the time window shown in Figure 4. One was measured during application of the RMP, while the other was measured after the RMP is turned off. In both cases, the amplitude of the $n=5$ mode has saturated, and a temperature structure is present. One noticeable difference between the two profiles is the width of the structure inside of $r/a=0.4$. The structure is narrower with the RMP applied. Such a narrowing has been observed in temperature profiles from multiple shots. The impact of a still-larger-amplitude RMP on the $T_e$ profile has yet to be explored.

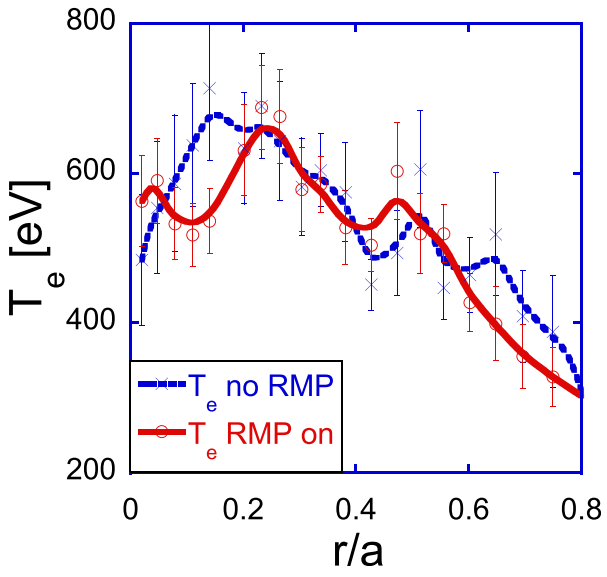


FIG. 8. Examples of electron temperature profiles during (red) and after (blue) application of a $b_r^{RMP}/B(a) \simeq 4\%$ magnetic perturbation. The two profiles are extracted from 25 and 30 ms in Figure 4.

## FIELD LINE TRACING RECONSTRUCTIONS

The data in the RMP impact on non-thermal and thermal electrons section suggest that the $m=1$ RMP may be changing the magnetic topology by reintroducing and/or intensifying magnetic stochasticity. To better understand this potential effect, we have reconstructed the magnetic topology for various cases with the MAL[54] field line tracing code. These reconstructions start with data from the 3D resistive-MHD code, DEBS.[55] Included are an axisymmetric equilibrium plus the eigenfunctions associated with the 11 largest resonant $m=1$ tearing modes, with $5 \le n \le 15$. The mode spectrum from DEBS is flat. Hence, to mock up the very peaked QSH mode spectrum, the amplitude of the $n=5$ component is increased 10-fold, matching the experiment.

To this is added the vacuum field associated with the external magnetic perturbation. Since the magnetic perturbation is produced at the narrow vertical cut in the conducting shell, the associated toroidal mode spectrum is broad. Hence, we include 50 $n$ harmonics, all with the same poloidal periodicity, amplitude, and radial profile. The radial profile is the vacuum solution to Ampere's law using the current flowing in each correction coil. The plasma response has been neglected, which is a common assumption.[56–58]

In Figure 9 are Poincaré plots produced over the poloidal cross section at the toroidal location of the vertical cut in the shell. The field line maps are similar at other toroidal locations. In all these reconstructions, each field line completes 1500 toroidal transits, which is the number of turns needed by an electron to achieve an energy above 20 keV in MST. In the top left plot (Figure 9(a)) is the case without an external magnetic perturbation. In one quadrant is a region of reduced stochasticity corresponding to the 3D structure. The Poincaré plot is similar to those reconstructed from experimental measurements of QSH plasmas with a single helical axis.[43] This result is also in agreement with previous field line tracing studies where a region of reduced stochasticity was observed in conjunction with QSH states.[59] On the top right (Figure 9(b)), a $m=1$ perturbation is applied with an amplitude $\delta b_t^{MP}/\delta b_t^{(1,5)} = 3\%$, where we are now normalizing each (1,n) component of the external perturbation to the amplitude of the internally resonant (1,5) mode, both quantities measured at the boundary. This perturbation causes a shrinking of the structure. On the lower left (Figure 9(c)), the $m=1$ perturbation is increased to $\simeq$13%, causing the structure to vanish. On the lower right (Figure 9(d)), an $m=3$ perturbation is applied with an amplitude of $\simeq$13% once again. Here, the $m=1$ structure remains largely unperturbed. Note that despite the fact that the perturbation applied is local, the effect on the stochasticity is observed at any toroidal position. This can be attributed to the fact that the level of stochasticity depends on the average magnetic energy of the perturbations rather than on their position.[60]

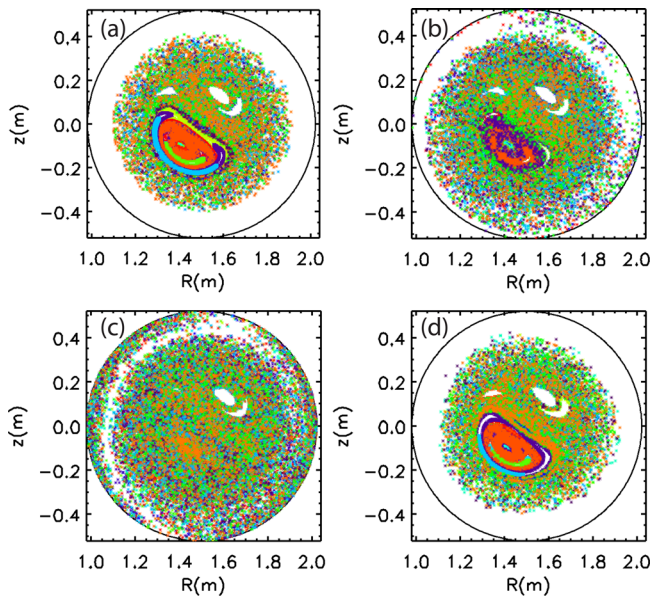


FIG. 9. Field line tracing reconstructions of QSH states with and without external magnetic perturbations. Case with no external perturbation on top left (a). Cases with weak ($\delta b_t^{MP}/\delta b_t^{(1,5)} = 3\%$) and strong ($\delta b_t^{MP}/\delta b_t^{(1,5)} = 13\%$) $m = 1$ perturbations on top right (b) and lower left (c), respectively. Case on lower right (d) is with strong ($\delta b_t^{MP}/\delta b_t^{(1,5)} = 13\%$) $m = 3$ perturbation.

To examine in more detail the variations of the radial width of the structure in Figure 9, we plot in Figure 10 the average magnetic field line wandering (*flw*) as a function of a field line's starting radius. The average magnetic field line wandering is computed by summing all the radial steps, normalized to the minor radius, a field line makes each toroidal transit and dividing by the number of transits. A field line starting in the stochastic region executes steps of random amplitude and direction. A value of $flw = 0.12$ has been established empirically as the threshold to identify the region where a field line is not free to move randomly. Therefore, the region where $flw < 0.12$ is considered to be the 3D structure. As the amplitude of the $m = 1$ perturbation increases, the radial width of the reduced-stochasticity region decreases, and, as expected, a $m = 3$ perturbation has essentially no impact on the radial width.

The variation with applied magnetic perturbation amplitude of the estimated width of the reduced-stochasticity

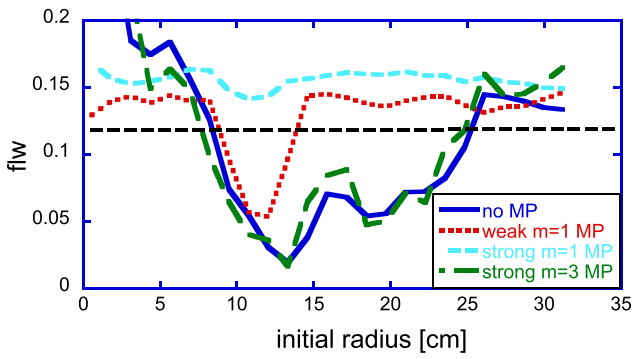


FIG. 10. Magnetic field lines wandering (*flw*) as a function of their initial radial location. The cases shown correspond to those in Figure 9. A value of $flw = 0.12$ is identified as the threshold to quantify the width of the reduced-stochasticity region.

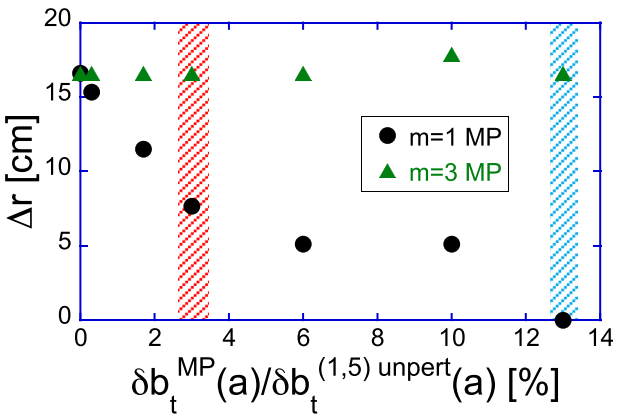


FIG. 11. Width of the area with $flw < 0.12$ as a function of the amplitude of the $m = 1$ and $m = 3$ perturbation. Red and blue shaded areas correspond to the weak and strong perturbations of Figures 9 and 10.

region is shown in greater detail in Figure 11 for both $m = 1$ and $m = 3$ perturbations. This width is that of the region with *flw* less than 0.12. The perturbation amplitudes for the cases shown in Figures 9 and 10 are highlighted. As expected, the radial width with the $m = 3$ perturbation is constant and equal to the case with zero external perturbation. On the other hand, the width decreases as the amplitude of the $m = 1$ perturbation increases.

The decrease in the x-ray flux versus $m = 1$ RMP amplitude is roughly consistent with the decrease in the size of the reduced-stochasticity region calculated with field-line tracing. The RMP amplitudes applied with the x-ray measurements were described in terms of $b_r^{RMP}/B(a)$, and the RMP amplitudes applied with the field-line-tracing calculations were described in terms of $\delta b_t^{MP}/\delta b_t^{(1,5)}$. But these two ratios describe very similar situations. $b_r^{RMP}$ is about two orders of magnitude larger than $\delta b_t^{MP}$, and $B(a)$ is about two orders of magnitude larger than $\delta b_t^{(1,5)}$.

## CONCLUSIONS

Magnetic perturbations are now used in MST to control the orientation of the helical equilibrium with respect to the diagnostics. Together with improvements in equilibrium reconstruction with V3FIT, this allowed us to build an ensemble of data to study thermal electrons in QSH plasmas. It revealed that the QSH state is characterized by the presence of an intermittent $T_e$ structure but also a more steady $n_e$ structure. Field line tracing reconstructions show that the 3D structure is a region of reduced stochasticity. They also show that as the amplitude of the $m = 1$ resonant magnetic perturbation increases, the reduced-stochasticity region shrinks and eventually vanishes. The suppression of the high-energy electrons also grows stronger as the perturbation amplitude increases.

That the high-energy electrons emerging during QSH could be confined in a region of reduced stochasticity associated with the helical structure was previously hypothesized based on field-line tracing with the ORBIT code.[37] Data in the present paper further support this hypothesis. The x-ray flux measured at a fixed location is shown to be larger with

the 3D structure in the detector's line of sight. Moreover, the x-ray flux depends strongly on the amplitude of the $m = 1$ RMP, which is shown to modify the region of reduced stochasticity.

## ACKNOWLEDGMENTS

This material is based upon work supported by the U.S. Department of Energy Office of Science, Office of Fusion Energy Sciences program under Award No. DE-FC02-05ER54814. MST data shown in this paper can be obtained in Ref. 61.

[1]T. E. Evans, R. A. Moyer, P. R. Thomas, J. G. Watkins, T. H. Osborne, J. A. Boedo, E. J. Doyle, M. E. Fenstermacher, K. H. Finken, R. J. Groebner, M. Groth, J. H. Harris, R. J. La Haye, C. J. Lasnier, S. Masuzaki, N. Ohyabu, D. G. Pretty, T. L. Rhodes, H. Reimerdes, D. L. Rudakov, M. J. Schaffer, G. Wang, and L. Zeng, Phys. Rev. Lett. **92**, 235003 (2004).
[2]B. Hudson, T. Evans, T. Osborne, C. Petty, P. Snyder, and E. Unterberg, Nucl. Fusion **50**, 045006 (2010).
[3]T. Evans, M. Fenstermacher, R. Moyer, T. Osborne, J. Watkins, P. Gohil, I. Joseph, M. Schaffer, L. Baylor, M. Becoulet, J. Boedo, K. Burrell, J. deGrassie, K. Finken, T. Jernigan, M. Jakubowski, C. Lasnier, M. Lehnen, A. Leonard, J. Lonnroth, E. Nardon, V. Parail, O. Schmitz, B. Unterberg, and W. West, Nucl. Fusion **48**, 024002 (2008).
[4]J. Canik, A. Sontag, R. Maingi, R. Bell, D. Gates, S. Gerhardt, H. Kugel, B. LeBlanc, J. Menard, S. Paul, S. Sabbagh, and V. Soukhanovskii, Nucl. Fusion **50**, 064016 (2010).
[5]W. Suttrop, T. Eich, J. C. Fuchs, S. Günter, A. Janzer, A. Herrmann, A. Kallenbach, P. T. Lang, T. Lunt, M. Maraschek, R. M. McDermott, A. Mlynek, T. Pütterich, M. Rott, T. Vierle, E. Wolfrum, Q. Yu, I. Zammuto, and H. Zohm (ASDEX Upgrade Team), Phys. Rev. Lett. **106**, 225004 (2011).
[6]W. Suttrop, L. Barrera, A. Herrmann, R. M. McDermott, T. Eich, R. Fischer, B. Kurzan, P. T. Lang, A. Mlynek, T. Pütterich, S. K. Rathgeber, M. Rott, T. Vierle, E. Viezzer, M. Willensdorfer, E. Wolfrum, I. Zammuto, and ASDEX Upgrade Team, Plasma Phys. Controlled Fusion **53**, 124014 (2011).
[7]Y. M. Jeon, J.-K. Park, S. W. Yoon, W. H. Ko, S. G. Lee, K. D. Lee, G. S. Yun, Y. U. Nam, W. C. Kim, J.-G. Kwak, K. S. Lee, H. K. Kim, and H. L. Yang (KSTAR Team), Phys. Rev. Lett. **109**, 035004 (2012).
[8]A. Kirk, I. T. Chapman, J. Harrison, Y. Liu, E. Nardon, S. Saarelma, R. Scannell, A. J. Thornton, and MAST Team, Plasma Phys. Controlled Fusion **55**, 015006 (2013).
[9]A. Kirk, I. Chapman, Y. Liu, P. Cahyna, P. Denner, G. Fishpool, C. Ham, J. Harrison, Y. Liang, E. Nardon, S. Saarelma, R. Scannell, A. Thornton, and MAST Team, Nucl. Fusion **53**, 043007 (2013).
[10]Y. Liang, H. Koslowski, P. Thomas, E. Nardon, S. Jachmich, A. Alfier, G. Arnoux, Y. Baranov, M. Becoulet, M. Beurskens, R. Coelho, T. Eich, E. D. L. Luna, W. Fundamenski, S. Gerasimov, C. Giroud, M. Gryaznevich, D. Harting, A. Huber, A. Kreter, L. Moreira, V. Parail, S. Pinches, S. Saarelma, O. Schmitz, and JET-EFDA Contributors, Nucl. Fusion **50**, 025013 (2010).
[11]Y. Liang, P. Lomas, I. Nunes, M. Gryaznevich, M. Beurskens, S. Brezinsek, J. Coenen, P. Denner, T. Eich, L. Frassinetti, S. Gerasimov, D. Harting, S. Jachmich, A. Meigs, J. Pearson, M. Rack, S. Saarelma, B. Sieglin, Y. Yang, L. Zeng, and JET-EFDA Contributors, Nucl. Fusion **53**, 073036 (2013).
[12]M. Lehnen, S. A. Bozhenkov, S. S. Abdullaev, and M. W. Jakubowski (TEXTOR Team), Phys. Rev. Lett. **100**, 255003 (2008).
[13]P. Grigull, K. McCormick, Y. Feng, A. Werner, R. Brakel, H. Ehmler, F. Gadelmeier, D. Hartmann, D. Hildebrandt, R. Jaenicke, J. Kisslinger, T. Klinger, R. Knig, D. Naujoks, H. Niedermeyer, N. Ramasubramanian, F. Sardei, F. Wagner, and U. Wenzel, J. Nucl. Mater. **313–316**, 1287 (2003).
[14]Y. Feng, F. Sardei, J. Kisslinger, P. Grigull, K. McCormick, D. Reiter, L. Giannone, R. Knig, N. Ramasubramanian, H. Thomsen, and U. Wenzel, Nucl. Fusion **45**, 89 (2005).
[15]M. Kobayashi, S. Masuzaki, I. Yamada, N. Tamura, Y. Feng, K. Sato, M. Goto, Y. Narushima, T. Akiyama, J. Miyazawa, M. Shoji, S. Morita, B. J. Peterson, H. Funaba, N. Ohyabu, K. Narihara, T. Morisaki, H. Yamada, A. Komori, LHD Experimental Group, and D. Reiter, Phys. Plasmas **17**, 056111 (2010).
[16]M. Kobayashi, S. Masuzaki, I. Yamada, Y. Narushima, C. Suzuki, N. Tamura, B. Peterson, S. Morita, C. Dong, N. Ohno, S. Yoshimura, Y. Feng, M. Goto, K. Sato, T. Akiyama, K. Tanaka, and LHD Experiment Group, Nucl. Fusion **53**, 093032 (2013).
[17]P. R. Brunsell, D. Yadikin, D. Gregoratto, R. Paccagnella, T. Bolzonella, M. Cavinato, M. Cecconello, J. R. Drake, A. Luchetta, G. Manduchi, G. Marchiori, L. Marrelli, P. Martin, A. Masiello, F. Milani, S. Ortolani, G. Spizzo, and P. Zanca, Phys. Rev. Lett. **93**, 225001 (2004).
[18]J. Drake, P. Brunsell, D. Yadikin, M. Cecconello, J. Malmberg, D. Gregoratto, R. Paccagnella, T. Bolzonella, G. Manduchi, L. Marrelli, S. Ortolani, G. Spizzo, P. Zanca, A. Bondeson, and Y. Liu, Nucl. Fusion **45**, 557 (2005).
[19]R. Paccagnella, S. Ortolani, P. Zanca, A. Alfier, T. Bolzonella, L. Marrelli, M. E. Puiatti, G. Serianni, D. Terranova, M. Valisa, M. Agostini, L. Apolloni, F. Auriemma, F. Bonomo, A. Canton, L. Carraro, R. Cavazzana, M. Cavinato, P. Franz, E. Gazza, L. Grando, P. Innocente, R. Lorenzini, A. Luchetta, G. Manduchi, G. Marchiori, S. Martini, R. Pasqualotto, P. Piovesan, N. Pomaro, P. Scarin, G. Spizzo, M. Spolaore, C. Taliercio, N. Vianello, B. Zaniol, L. Zanotto, and M. Zuin, Phys. Rev. Lett. **97**, 075001 (2006).
[20]S. Martini, M. Agostini, C. Alessi, A. Alfier, V. Antoni, L. Apolloni, F. Auriemma, P. Bettini, T. Bolzonella, D. Bonfiglio, F. Bonomo, M. Brombin, A. Buffa, A. Canton, S. Cappello, L. Carraro, R. Cavazzana, M. Cavinato, G. Chitarin, A. Cravotta, S. D. Bello, A. D. Lorenzi, L. D. Pasqual, D. Escande, A. Fassina, P. Franz, G. Gadani, E. Gaio, L. Garzotti, E. Gazza, L. Giudicotti, F. Gnesotto, M. Gobbin, L. Grando, S. Guo, P. Innocente, R. Lorenzini, A. Luchetta, G. Malesani, G. Manduchi, G. Marchiori, D. Marcuzzi, L. Marrelli, P. Martin, E. Martines, A. Masiello, F. Milani, M. Moresco, A. Murari, L. Novello, S. Ortolani, R. Paccagnella, R. Pasqualotto, S. Peruzzo, R. Piovan, P. Piovesan, A. Pizzimenti, N. Pomaro, M. Puiatti, G. Rostagni, F. Sattin, P. Scarin, G. Serianni, P. Sonato, E. Spada, A. Soppelsa, G. Spizzo, M. Spolaore, C. Taccon, C. Taliercio, D. Terranova, V. Toigo, M. Valisa, N. Vianello, P. Zaccaria, P. Zanca, B. Zaniol, L. Zanotto, E. Zilli, G. Zollino, and M. Zuin, Nucl. Fusion **47**, 783 (2007).
[21]S. Munaretto, B. E. Chapman, D. J. Holly, M. D. Nornberg, R. J. Norval, D. J. D. Hartog, J. A. Goetz, and K. J. McCollam, Plasma Phys. Controlled Fusion **57**, 104004 (2015).
[22]G. Papp, M. Drevlak, T. Fp, P. Helander, and G. I. Pokol, Plasma Phys. Controlled Fusion **53**, 095004 (2011).
[23]G. Papp, M. Drevlak, T. Fp, and G. I. Pokol, Plasma Phys. Controlled Fusion **54**, 125008 (2012).
[24]R. Lorenzini, E. Martines, P. Piovesan, D. Terranova, P. Zanca, M. Zuin, A. Alfier, D. Bonfiglio, F. Bonomo, A. Canton, S. Cappello, L. Carraro, R. Cavazzana, D. F. Escande, A. Fassina, P. Franz, M. Gobbin, P. Innocente, L. Marrelli, R. Pasqualotto, M. E. Puiatti, M. Spolaore, M. Valisa, N. Vianello, and P. Martin, Nat. Phys. **5**, 570 (2009).
[25]B. E. Chapman, "Direct diagnosis and parametric dependence of 3D helical equilibrium in the MST RFP, EX/P6-01," in *Proceedings IAEA Conference* (2012).
[26]J. Sarff, A. Almagri, J. Anderson, M. Borchardt, D. Carmody, K. Caspary, B. Chapman, D. D. Hartog, J. Duff, S. Eilerman, A. Falkowski, C. Forest, J. Goetz, D. Holly, J.-H. Kim, J. King, J. Ko, J. Koliner, S. Kumar, J. Lee, D. Liu, R. Magee, K. McCollam, M. McGarry, V. Mirnov, M. Nornberg, P. Nonn, S. Oliva, E. Parke, J. Reusch, J. Sauppe, A. Seltzman, C. Sovinec, H. Stephens, D. Stone, D. Theucks, M. Thomas, J. Triana, P. Terry, J. Waksman, W. Bergerson, D. Brower, W. Ding, L. Lin, D. Demers, P. Fimognari, J. Titus, F. Auriemma, S. Cappello, P. Franz, P. Innocente, R. Lorenzini, E. Martines, B. Momo, P. Piovesan, M. Puiatti, M. Spolaore, D. Terranova, P. Zanca, V. Belykh, V. Davydenko, P. Deichuli, A. Ivanov, S. Polosatkin, N. Stupishin, D. Spong, D. Craig, R. Harvey, M. Cianciosa, and J. Hanson, Nucl. Fusion **53**, 104017 (2013).
[27]S. Cappello and R. Paccagnella, Phys. Fluids B **4**, 611 (1992).
[28]J. M. Finn, R. Nebel, and C. Bathke, Phys. Fluids B **4**, 1262 (1992).
[29]S. Cappello and D. F. Escande, Phys. Rev. Lett. **85**, 3838 (2000).
[30]D. Bonfiglio, M. Veranda, S. Cappello, D. F. Escande, and L. Chacón, Phys. Rev. Lett. **111**, 085002 (2013).
[31]M. Veranda, D. Bonfiglio, S. Cappello, L. Chacón, and D. F. Escande, Plasma Phys. Controlled Fusion **55**, 074015 (2013).
[32]R. Paccagnella, Phys. Plasmas **21**, 032307 (2014).
[33]J.-H. Kim and P. W. Terry, Phys. Plasmas **19**, 122304 (2012).

[34]P. W. Terry and G. G. Whelan, Plasma Phys. Controlled Fusion **56**, 094002 (2014).
[35]R. N. Dexter, D. W. Kerst, T. W. Lovell, S. C. Prager, and J. C. Sprott, Fusion Technol. **19**, 131 (1991), available at http://www.ans.org/pubs/journals/fst/a_29322.
[36]J. D. Hanson, S. P. Hirshman, S. F. Knowlton, L. L. Lao, E. A. Lazarus, and J. M. Shields, Nucl. Fusion **49**, 075031 (2009).
[37]D. J. Clayton, B. E. Chapman, R. O'Connell, A. F. Almagri, D. R. Burke, C. B. Forest, J. A. Goetz, M. C. Kaufman, F. Bonomo, P. Franz, M. Gobbin, and P. Piovesan, Phys. Plasmas **17**, 012505 (2010).
[38]B. E. Chapman, R. Fitzpatrick, D. Craig, P. Martin, and G. Spizzo, Phys. Plasmas **11**, 2156 (2004).
[39]J. A. Reusch, M. T. Borchardt, D. J. Den Hartog, A. F. Falkowski, D. J. Holly, R. O'Connell, and H. D. Stephens, Rev. Sci. Instrum. **79**, 10E733 (2008).
[40]B. H. Deng, D. L. Brower, W. X. Ding, M. D. Wyman, B. E. Chapman, and J. S. Sarff, Rev. Sci. Instrum. **77**, 10F108 (2006).
[41]P. Franz, F. Bonomo, G. Gadani, L. Marrelli, P. Martin, P. Piovesan, G. Spizzo, B. E. Chapman, and M. Reyfman, Rev. Sci. Instrum. **75**, 4013 (2004).
[42]M. B. McGarry, P. Franz, D. J. Den Hartog, J. A. Goetz, M. A. Thomas, M. Reyfman, and S. T. A. Kumar, Rev. Sci. Instrum. **83**, 10E129 (2012).
[43]R. Lorenzini, D. Terranova, A. Alfier, P. Innocente, E. Martines, R. Pasqualotto, and P. Zanca, Phys. Rev. Lett. **101**, 025005 (2008).
[44]F. Auriemma, P. Zanca, W. F. Bergerson, B. E. Chapman, W. X. Ding, D. L. Brower, P. Franz, P. Innocente, R. Lorenzini, B. Momo, and D. Terranova, Plasma Phys. Controlled Fusion **53**, 105006 (2011).
[45]E. Martines, R. Lorenzini, B. Momo, D. Terranova, P. Zanca, A. Alfier, F. Bonomo, A. Canton, A. Fassina, P. Franz, and P. Innocente, Plasma Phys. Controlled Fusion **53**, 035015 (2011).
[46]W. F. Bergerson, F. Auriemma, B. E. Chapman, W. X. Ding, P. Zanca, D. L. Brower, P. Innocente, L. Lin, R. Lorenzini, E. Martines, B. Momo, J. S. Sarff, and D. Terranova, Phys. Rev. Lett. **107**, 255001 (2011).
[47]J. Hanson, D. Anderson, M. Cianciosa, P. Franz, J. Harris, G. Hartwell, S. Hirshman, S. Knowlton, L. Lao, E. Lazarus, L. Marrelli, D. Maurer, J. Schmitt, A. Sontag, B. Stevenson, and D. Terranova, Nucl. Fusion **53**, 083016 (2013).
[48]S. P. Hirshman and J. C. Whitson, Phys. Fluids **26**, 3553 (1983).
[49]J. Koliner, M. Cianciosa, J. Anderson, J. Hanson, B. Chapman, and J. Boguski, "3D equilibrium solutions for a current-carrying reversed-field pinch plasma with a close-fitting conducting shell," Phys. Plasmas (to be published).
[50]P. Franz, M. Gobbin, L. Marrelli, A. Ruzzon, F. Bonomo, A. Fassina, E. Martines, and G. Spizzo, Nucl. Fusion **53**, 053011 (2013).
[51]R. B. White and M. S. Chance, Phys. Fluids **27**, 2455 (1984).
[52]A. M. DuBois, J. D. Lee, and A. F. Almagri, Rev. Sci. Instrum. **86**, 073512 (2015).
[53]J. K. Anderson, W. Capecchi, S. Eilerman, J. J. Koliner, M. D. Nornberg, J. A. Reusch, J. S. Sarff, and L. Lin, Plasma Phys. Controlled Fusion **56**, 094006 (2014).
[54]B. F. Hudson, "Fast ion confinement in the reversed-field pinch," Ph.D. thesis, University of Wisconsin – Madison, 2006.
[55]D. Schnack, D. Barnes, Z. Mikic, D. S. Harned, and E. Caramana, J. Comput. Phys. **70**, 330 (1987).
[56]O. Schmitz, T. E. Evans, M. E. Fenstermacher, H. Frerichs, M. W. Jakubowski, M. J. Schaffer, A. Wingen, W. P. West, N. H. Brooks, K. H. Burrell, J. S. deGrassie, Y. Feng, K. H. Finken, P. Gohil, M. Groth, I. Joseph, C. J. Lasnier, M. Lehnen, A. W. Leonard, S. Mordijck, R. A. Moyer, A. Nicolai, T. H. Osborne, D. Reiter, U. Samm, K. H. Spatschek, H. Stoschus, B. Unterberg, E. A. Unterberg, J. G. Watkins, R. Wolf, and DIII-D and TEXTOR Teams, Plasma Phys. Controlled Fusion **50**, 124029 (2008).
[57]E. Nardon, P. Cahyna, S. Devaux, A. Kirk, A. Alfier, E. D. L. Luna, G. D. Temmerman, P. Denner, T. Eich, T. Gerbaud, D. Harting, S. Jachmich, H. Koslowski, Y. Liang, and Y. Sun, J. Nucl. Mater. **415**, S914 (2011).
[58]I. Chapman, M. Becoulet, T. Bird, J. Canik, M. Cianciosa, W. Cooper, T. Evans, N. Ferraro, C. Fuchs, M. Gryaznevich, Y. Gribov, C. Ham, J. Hanson, G. Huijsmans, A. Kirk, S. Lazerson, Y. Liang, I. Lupelli, R. Moyer, C. Nhrenberg, F. Orain, D. Orlov, W. Suttrop, D. Yadykin, ASDEX Upgrade, DIII-D, MAST and NSTX Teams, and EFDA-JET Contributors, Nucl. Fusion **54**, 083006 (2014).
[59]D. F. Escande, R. Paccagnella, S. Cappello, C. Marchetto, and F. D'Angelo, Phys. Rev. Lett. **85**, 3169 (2000).
[60]F. D'Angelo and R. Paccagnella, Plasma Phys. Controlled Fusion **38**, 313 (1996).
[61]See supplementary material at http://dx.doi.org/10.1063/1.4943524 for the digital format of the data shown in this paper.